Stability Analysis Method for Three-Phase Multi-Functional Grid-Connected Inverters With Unbalanced Local Loads Considering the Active Imbalance Compensation

WEI JIN[iD], YONGLI LI, GUANGYU SUN[iD], XIAOLONG CHEN[iD], AND YAN GAO

Key Laboratory of Smart Grid of Ministry of Education, Tianjin University, Tianjin 300072, China

Corresponding author: Xiaolong Chen (promising1207@163.com)

ABSTRACT This paper proposes a small-signal stability analysis method for the three-phase multi-functional grid-connected inverter (MFGCI) system with an unbalanced local load based on impedance modeling. To attenuate the imbalance introduced by the local load, a modified power quality-compensation algorithm for the MFGCI based on the conservative power theory is proposed and incorporated into the stability analysis. The impedance model of the three-phase system is developed by adopting the complex space vector method to simplify the stability analysis process in this paper. In addition, based on the proposed impedance model and stability analysis, it is proven that the unbalanced local load can affect the stability of the system when the grid-impedance is not negligible. Furthermore, the adoption of the active imbalance compensation can reshape the impedance characteristics of the unbalanced system and improve the stability. The accuracy of the proposed impedance model, and the stability analysis results are verified by the simulation and experimental results.

INDEX TERMS Multi-functional grid-connected inverter, three-phase imbalance compensation, impedance model, small-signal stability.

I. INTRODUCTION

Three-phase voltage-source grid-connected inverters are widely used in grid-integrated distributed generations (DGs). Due to their high flexibility and controllability, the grid-connected inverters are applied not only to transmit the active power of DGs but also to help achieve the compensation of power quality problems (e.g., harmonic or three-phase imbalance distortion). Thus, the concept of the multi-functional grid-connected inverter (MFGCI) has been proposed [1]. When the MFGCI is connected to the grid, most of its functions are realized by controlling the output currents. Therefore, the current control loop of the grid-connected inverter has been the research focus of late [2]–[4]. However, previous studies indicate that the current control loop can cause oscillation of the grid-connected inverter in weak grid conditions [5]. To study the small-signal stability issue, impedance (admittance) models, both in synchronously rotating frame and stationary frame, have been proposed, taking into account the current control loop and the phase-locked loop (PLL) [6]–[8]. The method to establish the impedance model in phase-domain was proposed [8]. Then, the complex space vector method was adopted to derive the impedance model [9]. The proposed impedance models are mostly matrix-based, due to the coupling between the d and q axes or different sequence components. To simplify the stability analysis process, a single-input-single-output (SISO) equivalent impedance model was proposed considering the coupling between the positive-sequence and negative-sequence components of grid-connected inverter systems [10].

Besides the current control loop, a previous study proved that the three-phase imbalance of the grid-impedance can also reduce the stability of the grid-connected inverter system based on the impedance analysis [11]. However, in practice, the DGs are commonly connected to the distribution grid with local loads. Thus, the imbalance of the system can

also be caused by the unbalanced local load. In addition, to compensate for the imbalance distortion, the active compensation algorithm is integrated into the control system of the MFGCI to extract the imbalance load current component as the reference value for the output-current [12]. Theoretically, by tracking the calculated reference value, the unbalanced load current can be offset by the output-current of the MFGCI. Thus, the three-phase balanced current of the point of common coupling (PCC) can be achieved [13].

From the viewpoint of system impedance model, it can be considered that the active compensation changes the three-phase unbalanced feature of the system output impedance to the three-phase balanced feature. Moreover, the equivalent impedance of the compensated system is directly related to the current control loop and the imbalance compensation algorithm of the MFGCI. Accordingly, the small-signal stability of the three-phase system can be affected by not only the unbalanced local load but also the adoption of the active imbalance compensation. However, existing impedance modeling methods do not consider adopting the active imbalance compensation algorithm. The small-signal stability study for the MFGCI system with unbalanced local load is also inadequate.

To study this issue, the impedance model for the three-phase system including the MFGCI and the unbalanced local load is proposed in this paper. By adopting the complex space vector method, the positive-sequence and negative-sequence SISO impedance models previously proposed [10] are unified. Furthermore, the modified imbalance compensation algorithm based on the conservative power theory (CPT) is integrated into the proposed impedance model. By adopting the compensation algorithm, the imbalance load current can be extracted in phase-domain without the *dq* transformation [14]. Moreover, the compensation current generated by the compensation algorithm can exclude the balanced reactive component of the load current, which helps to save the compensation capacity [15]. Based on the proposed impedance model, the detailed stability analysis for the three-phase system is performed in this paper taking into account the influence of the grid-impedance. The analysis verified that the imbalance of the local load can affect the stability of the system. The study also proved that the adoption of the proposed CPT-based compensation algorithm can decrease the imbalance of the system by reshaping the equivalent impedance of the unbalanced load. Therefore, the stability of the system can be enhanced. Both the simulation and experimental results confirmed the accuracy of the proposed model and the stability analysis results.

This paper is organized as follows. In Section II, based on the complex space vector method, the three-phase system impedance model is built considering the MFGCI with an LCL filter and the unbalanced local load. In Section III, the imbalance compensation algorithm based on the CPT is integrated into the model to derive the equivalent impedance of the compensated system. The verification of the proposed model is also presented. The stability analysis of the system taking the grid-impedance into account is performed in Section IV. Section V presents the experimental results. Finally, the conclusions drawn from this work are given in Section VI.

II. SMALL-SIGNAL IMPEDANCE MODEL OF THE THREE-PHASE GRID-CONNECTED INVERTER SYSTEM WITH THE UNBALANCED LOCAL LOAD
A. TOPOLOGY OF THE THREE-PHASE SYSTEM AND IMPEDANCE MODEL OF THE UNBALANCED LOAD
When the MFGCI and the unbalanced local load are connected to the same PCC, the topology of the three-phase system is illustrated in Fig. 1.
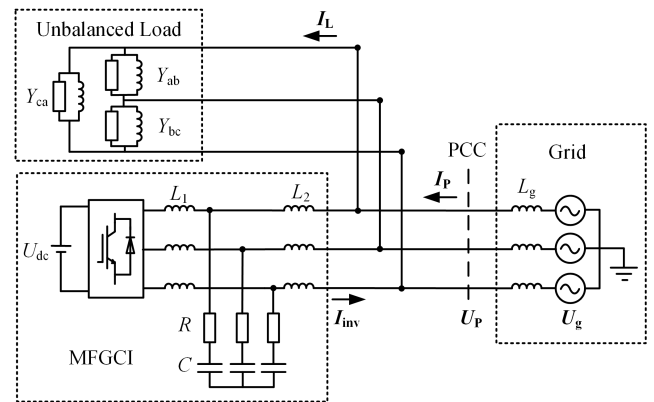

**FIGURE 1.** Topology of the three-phase system with the unbalanced local load and the MFGCI.

As illustrated in Fig. 1, The LCL filter is adopted in the MFGCI to eliminate the high-frequency harmonic caused by the pulse-width modulation (PWM). The LCL filter is composed of the inverter-side inductor L_1, the grid-side inductor L_2, and the capacitor C. R is the damping resistor. The three-phase delta-connected load is connected to the same PCC with the MFGCI. To simulate the active and reactive power consumption, each phase-to-phase load is considered a resistor with a parallel inductor. The admittances of the loads are denoted as Y_{ab}, Y_{bc}, and Y_{ca}.

To simplify the analysis, the complex space vector method is adopted to derive the impedance model of the three-phase system. The three-phase quantities in a three-phase system can be represented as complex space vectors [16]. In addition, the rotating direction of the positive-sequence quantity at the fundamental-frequency is defined as the positive direction. Considering the existence of a small-signal perturbation, the three-phase voltage of the PCC $U_{\mathbf{P}}$ can be expressed as:

$$\begin{aligned}
\boldsymbol{U_{\mathbf{P}}} &= \boldsymbol{U_0} + \boldsymbol{U_e} \\
&= U_0 e^{j\omega_0 t} + U_e e^{j(\omega_e t + \theta_e)} \quad \omega_e \in (-\infty, +\infty) \quad (1)
\end{aligned}$$

where $\boldsymbol{U_0}$ is the three-phase voltage at the fundamental-frequency; ω_0 is the fundamental angular frequency; U_0 is the magnitude of $\boldsymbol{U_0}$; $\boldsymbol{U_e}$ is the three-phase perturbation voltage; ω_e is the angular frequency of $\boldsymbol{U_e}$; the magnitude of the

perturbation voltage is denoted by U_e; θ_e is the initial phase of the perturbation voltage. As a small-signal perturbation, the magnitude of the perturbation voltage meets the condition $U_e \ll U_0$. By adopting the complex space vector method, a positive-sequence perturbation voltage can be expressed as U_e at a positive angular frequency ($\omega_e > 0$) and a negative-sequence perturbation voltage can be expressed as U_e at a negative angular frequency ($\omega_e < 0$). Based on this definition of the complex space vector, the components of U_P are depicted in Fig. 2.
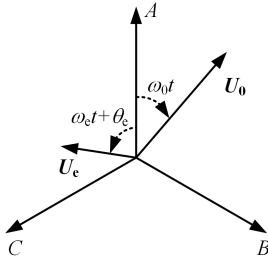
FIGURE 2. Complex space vector diagram in *abc*-frame for the three-phase voltage of the PCC. (Clockwise direction is the positive direction. In the presented case, $\omega_0 > 0$ and $\omega_e < 0$.)

When a negative-sequence perturbation is added to the three-phase voltage of the PCC, the complex space vectors of U_0 and U_e can be represented as shown in Fig. 2. It shows that by introducing the concept of negative angular frequency, the expressions for positive-sequence and negative-sequence quantities can be unified.

When the unbalanced load is connected at the PCC under the U_P with small-signal perturbation, the three-phase load current I_L can be expressed as:

$$I_L = \begin{cases} I_{L0} = I_{L0}e^{j(\omega_0 t + \theta_{L0})} \\ I_{LN0} = I_{LN0}e^{j(-\omega_0 t + \theta_{LN0})} \\ I_{Le} = I_{Le}e^{j(\omega_e t + \theta_{Le})} \\ I_{LNe} = I_{LNe}e^{j(-\omega_e t + \theta_{LNe})} \end{cases} \quad (2)$$

Under U_0 and U_e, I_L includes I_{L0} at the frequency ω_0 and I_{Le} at the frequency ω_e. Moreover, due to the imbalance of the load, the current components I_{LN0} at the frequency $-\omega_0$ and I_{LNe} at the frequency $-\omega_e$ also exist in I_L. I_{L0}, I_{LN0}, I_{Le}, and I_{LNe} represent the magnitudes of the space vectors I_{L0}, I_{LN0}, I_{Le} and I_{LNe}, while the initial phases of the space vectors are represented by θ_{L0}, θ_{LN0}, θ_{Le}, and θ_{LNe}, respectively.

According to the small-signal linearization method, the voltage and current components related to the small-signal perturbation is considered. Therefore, an equivalent small-signal impedance model in the frequency-domain for the three-phase unbalanced load can be derived and is depicted in Fig. 3.

In the frequency-domain, the expression of the perturbation voltage U_e can be derived as:

$$U_e(\omega) = 2\pi U_e e^{j\theta_e}\delta(\omega - \omega_e) \quad (3)$$
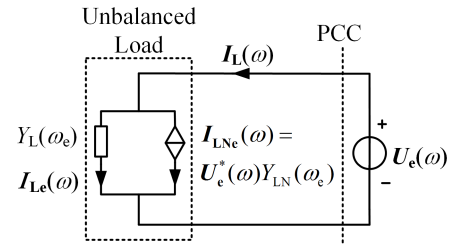
FIGURE 3. Small-signal Impedance model for the three-phase unbalanced load.

The load current in the frequency-domain $I_L(\omega)$ under $U_e(\omega)$ can be expressed as:

$$I_L(\omega) = \begin{cases} I_{Le}(\omega) = 2\pi I_{Le}e^{j\theta_{Le}}\delta(\omega - \omega_e) \\ I_{LNe}(\omega) = 2\pi I_{LNe}e^{j\theta_{LNe}}\delta(\omega + \omega_e) \end{cases} \quad (4)$$

According to the space vectors of the three-phase load current shown in (4), the three-phase load can be modeled as a balanced admittance (or impedance) in parallel with a voltage-controlled-current-source. The equivalent balanced admittance of the load at the frequency ω_e is represented as $Y_L(\omega_e)$ in Fig. 3. Additionally, $Y_L(\omega_e)$ can be derived based on the expressions of the phase-to-phase load admittances as:

$$Y_L(\omega_e) = \frac{I_{Le}(\omega)}{U_e(\omega)} = Y_{ab}(\omega_e) + Y_{bc}(\omega_e) + Y_{ca}(\omega_e) \quad (5)$$

As shown in (5), the expressions of the phase-to-phase load admittances in the frequency-domain at ω_e are represented as $Y_{ab}(\omega_e)$, $Y_{bc}(\omega_e)$, and $Y_{ca}(\omega_e)$.

The imbalance of the local load produces $I_{LNe}(\omega)$ at the frequency $-\omega_e$. Since $I_{LNe}(\omega)$ is at the different frequency from the $U_e(\omega)$, the voltage-controlled-current-source is used to represent the relation between the current and the external excitation voltage. In addition, the coupled-admittance $Y_{LN}(\omega_e)$ is defined to describe the relationship between $I_{LNe}(\omega)$ and $U_e(\omega)$. The expression of $Y_{LN}(\omega_e)$ can be derived as:

$$Y_{LN}(\omega_e) = \frac{I_{LNe}(\omega)}{U_e^*(\omega)}$$
$$= -\left[e^{j\frac{4\pi}{3}}Y_{ab}(\omega_e) + Y_{bc}(\omega_e) + e^{j\frac{2\pi}{3}}Y_{ca}(\omega_e)\right]^* \quad (6)$$

where U_e^* is the conjugate vector of U_e. Based on (5) and (6), the proposed small-signal impedance model can be directly derived based on the expressions of the actual loads in the frequency-domain.

B. IMPEDANCE MODEL OF THE UNBALANCED THREE-PHASE SYSTEM WITH THE MFGCI

When the MFGCI is connected to the grid at the same PCC as the unbalanced load, the small-signal impedance model of the three-phase system can be represented as depicted in Fig. 4.

As illustrated in Fig. 4, the Norton equivalent model of the grid-connected inverter [6] is adopted. $I_{inv}(\omega)$ is the three-phase output-current of the MFGCI in the frequency-domain.
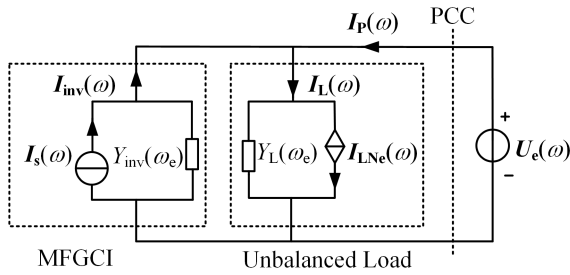
FIGURE 4. Small-signal Impedance model for the three-phase system including the unbalanced load and the MFGCI.

The current-source is an equivalent of the current control loop of the MFGCI. $I_s(\omega)$ is the output-current of the equivalent current-source. $Y_{inv}(\omega_e)$ is the equivalent admittance which represents the interference from the perturbation voltage U_e. The expression of the equivalent impedance can be derived based on the complex transfer functions [16] of the control system.
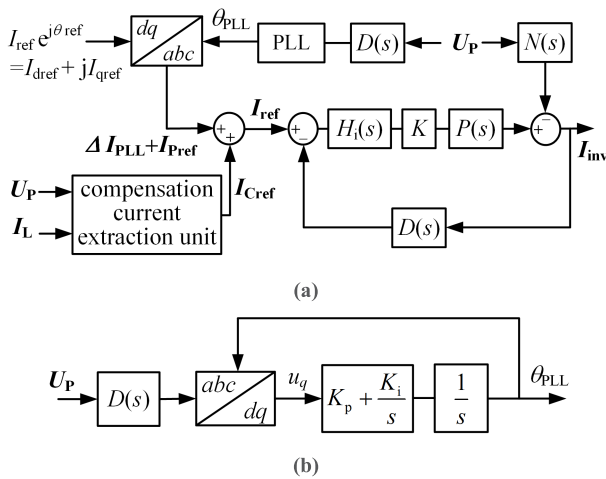

(a)

(b)

FIGURE 5. Block diagrams for the control system of the MFGCI. (a) The diagram for the current control scheme. (b) The diagram for the PLL.

As shown in Fig. 5(a), the current control scheme in the stationary frame is adopted in the MFGCI. I_{dref} and I_{qref} are the active-power current reference and the reactive-power current reference, respectively, in the dq-frame. The I_{dref} and I_{qref} are considered as constants in small-signal analysis. Thus, the power current reference can be expressed in complex form as $I_{ref}e^{j\theta ref}$. To achieve power transmission and power quality compensation, the output-current reference I_{ref} includes two separate parts. One is the power current reference which is derived from $I_{ref}e^{j\theta ref}$ by dq-abc transformation. The other is the compensation current reference I_{Cref}, which is calculated based on I_L and U_P. $H_i(s)$ is the transfer function of the current controller. K represents the PWM gain. $D(s)$ is the transfer function for sampling delay and can be expressed as:

$$D(s) = \frac{1 - e^{-T_s s}}{T_s s} e^{-T_s s} \qquad (7)$$

where T_s is the sampling period of the control system. $P(s)$ is the transfer function of the LCL filter, and can be expressed as:

$$P(s) = \frac{CRs + 1}{CL_1 L_2 s^3 + CR(L_1 + L_2)s^2 + (L_1 + L_2)s} \qquad (8)$$

Based on $H_i(s)$, $D(s)$, and $P(s)$, the closed-loop transfer function of the current control loop can be derived as:

$$G(s) = \frac{KH_i(s)P(s)}{1 + KH_i(s)P(s)D(s)} \qquad (9)$$

According to Fig. 5(a), when U_P contains the perturbation voltage U_e, the interference current component at the frequency ω_e can be introduced in I_{inv} through $N(s)$ and PLL. $N(s)$ can be derived as:

$$N(s) = \frac{CL_1 s^2 + CRs + 1}{CL_1 L_2 s^3 + CR(L_1 + L_2)s^2 + (L_1 + L_2)s} \qquad (10)$$

As illustrated in Fig. 5(b), the synchronous reference frame phase-locked loop (SRF-PLL) is adopted to calculate the phase of U_0. However, the perturbation voltage U_e can cause disturbance to the calculated phase θ_{PLL} [8]. Therefore, the interference ΔI_{PLL} is introduced to the output-current reference by the dq-abc transformation based on θ_{PLL}. According to the PLL small-signal model previously proposed [8], [9], the expression of ΔI_{PLL} in the frequency-domain can be expressed as:

$$\Delta I_{PLL}(\omega) = \frac{1}{2} I_{ref} e^{j\theta ref} \left[F(s - j\omega_0)D(s) \right] \Big|_{s=j\omega_e} U_e(\omega) \qquad (11)$$

where

$$F(s) = \frac{K_p s + K_i}{s^2 + U_0(K_p s + K_i)} \qquad (12)$$

In (12), K_p and K_i are the proportional-coefficient and the integral-coefficient of the SRF-PLL, respectively.

Based on the above-mentioned analysis, the Norton equivalent model presented in Fig. 4 for the grid-connected inverter can be expressed as:

$$I_{inv}(\omega) = I_s(\omega) - Y_{inv}(\omega_e)U_e(\omega) \qquad (13)$$

$I_s(\omega)$ can be further expanded as:

$$I_s(\omega) = G(s)|_{s=j\omega} \left[I_{Pref}(\omega) + I_{Cref}(\omega) \right] \qquad (14)$$

where $I_{Pref}(\omega)$ is the frequency-domain expression for power current reference in abc-frame and can be expressed as $2\pi I_{ref}e^{j\theta ref}\delta(\omega - \omega_0)$. Moreover, the equivalent admittance $Y_{inv}(\omega_e)$ can be derived based on (7), (9), (10), and (11) as

$$Y_{inv}(\omega_e) = \left[\frac{N(s)}{1 + KH_i(s)P(s)D(s)} \right. $$
$$\left. - \frac{I_{ref}e^{j\theta ref}}{2} F(s - j\omega_0)D(s)G(s) \right] \Bigg|_{s=j\omega_e} \qquad (15)$$

In summary, based on (5), (6), (14), and (15), the expressions of the different components which compose the small-signal model shown in Fig. 4 can be obtained.

III. SMALL-SIGNAL IMPEDANCE MODEL CONSIDERING THE ACTIVE IMBALANCE COMPENSATION ALGORITHM

The small-signal model proposed in Section II reveals the relationship between the compensation current reference I_{Cref} and the inverter output-current I_{inv}. As shown in Fig. 5(a), I_{Cref} is calculated based on the load current I_L. Therefore, the coupling between the MFGCI and the unbalance load is introduced by the compensation current extraction unit.

In this Section, the compensation current extraction algorithm in the stationary frame is proposed based on the CPT. By adopting the complex space vector method, the expression of I_{Cref} is derived based on the expression of I_L, considering the load topology presented in Fig. 1. Thus, the equivalent impedances for the compensated unbalanced load are derived. Furthermore, the small-signal impedance model for the three-phase system with the MFGCI and the compensated unbalanced load is confirmed based on the impedance measurement.

A. COMPENSATION CURRENT EXTRACTION ALGORITHM BASED ON THE CPT

The CPT provides a method to decompose the current components in the stationary frame, and has been successfully applied for harmonic current and imbalance current compensation [12]–[14]. In this study, the CPT-based compensation current extraction algorithm is adopted to extract the unbalanced load current. Taking the existence of the perturbation voltage U_e into account, several modifications are made to the extraction algorithm. The block diagram for the proposed algorithm is presented in Fig. 6, based on the complex space vector method.

As shown in Fig. 6(a), I_{ba} and I_{br} are the equivalent balanced active current and the equivalent balanced reactive current, respectively, calculated based on the CPT. The compensation current reference I_{Cref} can be obtained by eliminating I_{ba} and I_{br} from I_{Ls}. I_{Ls} is the sampling value of the load current I_L. The calculation process of G_b and B_b is shown in Fig. 6(b).

Since the sampling period $T_s \ll T_0$, the delay effect of sampling at ω_0 and $-\omega_0$ can be neglected. Only the sampling values at ω_e and $-\omega_e$ are affected by the sampling delay $D(s)$. Thus, based on (7), the sampling value of U_P can be expressed as:

$$U_{Ps} = \begin{cases} U_0 \\ U_{es} = D(s)|_{s=j\omega_e} U_e \end{cases} \quad (16)$$

The sampling value of I_L can be expressed as:

$$I_{Ls} = \begin{cases} I_{L0} \\ I_{LN0} \\ I_{Les} = D(s)|_{s=j\omega_e} I_{Le} \\ I_{LNes} = D(s)|_{s=-j\omega_e} I_{LNe} \end{cases} \quad (17)$$

Based on the CPT, the unbiased time integral for the periodic quantity x (the period of x is T.) is defined by (18) to
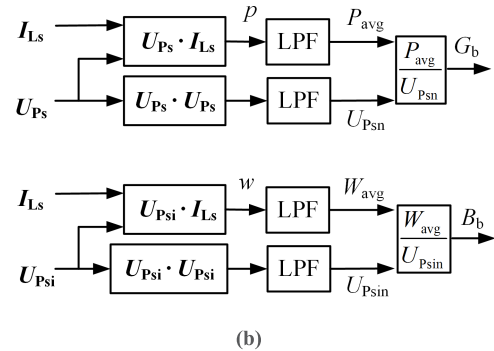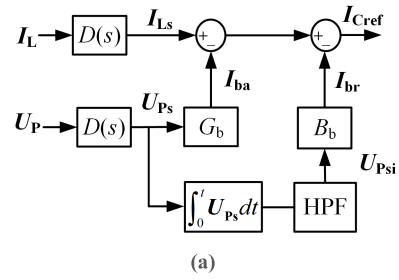

(a)

(b)

FIGURE 6. Block diagrams of the compensation current extraction algorithm based on the CPT. (a) The process for the calculation of I_{Cref}. (b) The process for the calculation of G_b and B_b.

calculate the reactive power [14].

$$x_i = x_f - \bar{x}_f$$
$$= \int_0^t x(\tau)d\tau - \frac{1}{T}\int_0^T x_f dt \quad (18)$$

Thus, the unbiased time integral for a complex space vector $X = X e^{j(\omega t + \theta)}$ can be derived as:

$$X_i = X_f - \bar{X}_f$$
$$= \left[(X/j\omega) - Xe^{j\theta}/j\omega\right] - \left[-Xe^{j\theta}/j\omega\right]$$
$$= X/j\omega \quad (19)$$

According to (18) and (19), the unbiased time integral can be achieved by eliminating the initial value from the ordinary time integral result. For a periodic quantity, the initial value of the ordinary time integral is constant and can be obtained by calculating the average value [17]. However, the period of the perturbation voltage U_e is uncertain in practice. Accordingly, as illustrated in Fig 6(a), the high-pass-filter (HPF) with low cutoff-frequency is adopted to eliminate the initial value of the ordinary integral result. Thus, the unbiased time integral result for U_{Ps} can be derived as:

$$U_{Psi} = U_{0i} + U_{esi} = U_0/j\omega_0 + U_{es}/j\omega_e \quad (20)$$

According to the CPT, the instantaneous active power p is defined as the inner product between U_{Ps} and I_{Ls}. The instantaneous reactive power w is defined as the inner product between U_{Psi} and I_{Ls} [14]. The p and w can be expressed as:

$$p = (U_0 + U_{es}) \bullet (I_{L0} + I_{LN0} + I_{Les} + I_{LNes})$$
$$w = (U_{0i} + U_{esi}) \bullet (I_{L0} + I_{LN0} + I_{Les} + I_{LNes}) \quad (21)$$

According to the definition of the inner product, the result of an inner product between two complex space vectors at the same frequency is constant. The result of an inner product between two complex space vectors at different frequencies is a sinusoidal quantity. To obtain the average active power P_{avg} and average reactive power W_{avg}, the low-pass-filter (LPF) is adopted to eliminate the sinusoidal quantities. Since the cutoff-frequency of the LPF is set close to 0 rad/s, the expressions for P_{avg} and W_{avg} can be expressed as:

$$P_{avg} = U_0 \bullet I_{L0} + U_{es} \bullet I_{Les}$$
$$W_{avg} = U_{0i} \bullet I_{L0} + U_{esi} \bullet I_{Les} \quad (22)$$

The same method is used to obtain U_{Psn} and U_{Psin} as illustrated in Fig. 6(b). The expressions can be derived as:

$$U_{Psn} = U_0 \bullet U_0 + U_{es} \bullet U_{es} = U_0^2 + U_{es}^2$$
$$U_{Psin} = U_{0i} \bullet U_{0i} + U_{esi} \bullet U_{esi} = U_{0i}^2 + U_{esi}^2 \quad (23)$$

According to the model of the unbalanced load presented in Section II.A, the load current components at the frequency ω_0 and ω_e can be expressed as $I_{L0} = Y_L(\omega_0) U_0$ and $I_{Le} = Y_L(\omega_e) U_e$, respectively. According to the load topology shown in Fig. 1, $Y_L(\omega)$ can be derived based on (5) as:

$$Y_L(\omega) = G_L + jB_L / \omega \quad (24)$$

where

$$G_L = 1/R_{ab} + 1/R_{bc} + 1/R_{ca}$$
$$B_L = -\left(1/L_{ab} + 1/L_{bc} + 1/L_{ca}\right) \quad (25)$$

Based on the calculation process shown in Fig. 6(b), G_b and B_b can be derived according to (22)-(25) and the expressions of I_{L0} and I_{Le} as:

$$G_b = G_L \quad B_b = -B_L \quad (26)$$

Therefore, the compensation current reference I_{Cref} can be derived as:

$$I_{Cref} = I_{Ls} - G_b U_{Ps} - B_b U_{Psi}$$
$$= I_{LN0} + I_{LNes} \quad (27)$$

It is revealed that the CPT-based compensation current extraction algorithm can extract the load current components at the frequency $-\omega_0$ and $-\omega_e$ which are caused by the imbalance of the load.

B. SMALL-SIGNAL IMPEDANCE MODEL FOR THE COMPENSATED UNBALANCED LOAD

According to the Norton model of the MFGCI, the compensation current produced by the MFGCI can be derived based on the expression of I_{Cref}. By integrating the compensation current into the model of the unbalanced load, the small-signal impedance model for the equivalent compensated load can be derived as shown in Fig. 7. Based on the small-signal linearization method, the components related to the small-signal
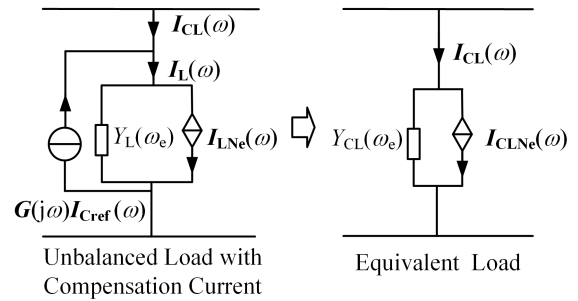

FIGURE 7. Small-signal Impedance model for the unbalanced load compensated by the MFGCI.

perturbation voltage are used to drive the equivalent admittances of the compensated load. Accordingly, the current of the equivalent load $I_{CL}(\omega)$ can be derived based on (27) as:

$$I_{CL}(\omega) = \begin{cases} I_{CLe}(\omega) = I_{Le}(\omega) \\ I_{CLNe}(\omega) = [1 - G(s)D(s)]|_{s=-j\omega_e} I_{LNe}(\omega) \end{cases} \quad (28)$$

Thus, the equivalent admittances for the compensated load can be derived based on (5) and (6) as:

$$Y_{CL}(\omega_e) = \frac{I_{CLe}(\omega)}{U_e(\omega)} = Y_L(\omega_e) \quad (29)$$

$$Y_{CLN}(\omega_e) = \frac{I_{CLNe}(\omega)}{U_e^*(\omega)}$$
$$= [1 - G(s)D(s)]|_{s=-j\omega_e} Y_{LN}(\omega_e) \quad (30)$$

According to (29) and (30), the adoption of the proposed compensation algorithm changes the characteristic of the coupled-admittance $Y_{LN}(\omega_e)$, which is determined by the imbalance of the load. The equivalent balanced admittance $Y_L(\omega_e)$ is not affected by the compensation.

C. VERIFICATION FOR THE SMALL-SIGNAL MODEL BASED ON IMPEDANCE MEASUREMENT

According to the theoretical analysis in Section II and III, the mathematical expressions of the small-signal model are derived considering the active imbalance compensation. To verify the accuracy of the proposed model, the impedance (admittance) measurement is performed in the MATLAB/Simulink environment. The topology for the measurement system is presented in Fig. 8.
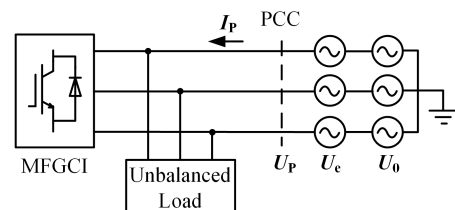

FIGURE 8. Diagram of the system for impedance measurement.

Parameter	Value
inverter-side inductance of the LCL filter L_1	0.9mH
grid-side inductance of the LCL filter L_2	0.1mH
capacitance of the LCL filter C	100uF
damping resistance of the LCL filter R	1Ω
PWM gain K	225
sampling period for the control system T_s	10^{-4}s
cut-off frequency of HPF	5Hz
cut-off frequency of LPF	5Hz
proportional coefficient of PLL K_p	11
integral coefficient of PLL K_i	100
active current reference I_d	30A
reactive current reference I_q	0A
load resistance between phase A and B R_{ab}	10Ω
load inductance between phase A and B L_{ab}	36mH
load inductance between phase B and C L_{bc}	36mH
load inductance between phase C and A L_{ca}	36mH

As illustrated in Fig. 8, the small-signal perturbation voltage U_e is in series with U_0. Based on the measured value of the current at the PCC I_P, the component of I_P at the frequency ω_e (represented as I_{Pe}) and the component of I_P at the frequency $-\omega_e$ (represented as I_{PNe}) can be obtained.

According to the small-signal model presented in Fig. 4, the admittance and coupled-admittance of the three-phase system under the perturbation voltage U_e can be obtained based on the values of I_{Pe}, I_{PNe}, and U_e, and can be expressed as:

$$Y_{inv}(\omega_e) + Y_L(\omega_e) = I_{Pe}/U_e$$
$$Y_{LN}(\omega_e) = I_{PNe}/U_e^* \qquad (31)$$

In addition, when the imbalance compensation algorithm is adopted, $Y_{inv}(\omega_e) + Y_{CL}(\omega_e)$ and $Y_{CLN}(\omega_e)$ can also be measured based on (31).

In the simulation, the fundamental frequency is 50Hz. $U_0 = 100$V and U_e is set as $0.1U_0$. The load resistor is only connected between phase A and phase B to simulate the imbalance of the system. The main parameters of the MFGCI and the unbalanced load are listed in Table I.

The multi-parallel proportional-resonant (PR) controller is commonly used to realize the current control in the ordinary grid-connected inverter and the MFGCI [2], [15], [18]. Thus, the multi-parallel PR controller is adopted in the system as current controller $H_i(s)$ and can be expressed as

$$H_i(s) = K_p + \sum_{i=1,3,5,7} \frac{2K_{hi}\omega_{ci}s}{s^2 + 2\omega_{ci}s + \omega_i^2} \qquad (32)$$

The parameters for $H_i(s)$ are $K_p = 0.011$; $K_{h1} = 0.35$, $\omega_1 = 100\pi$, $\omega_{c1} = 2$; $K_{h3} = 0.3$, $\omega_3 = 300\pi$, $\omega_{c3} = 2$; $K_{h5} = 0.3$, $\omega_5 = 500\pi$, $\omega_{c5} = 2$; $K_{h7} = 0.3$, $\omega_7 = 700\pi$, $\omega_{c7} = 2$.

The values of the admittances at variable frequencies can be obtained using the measurement system presented in Fig. 8. To verify the accuracy of the proposed small-signal, the measured values of the admittances are compared with the calculated values based on the formulas presented

in Section II and III. Additionally, the admittances considering the imbalance compensation are also compared with the admittances without the imbalance compensation to verify the effectiveness for the proposed compensation algorithm. The results are presented in Fig. 9.
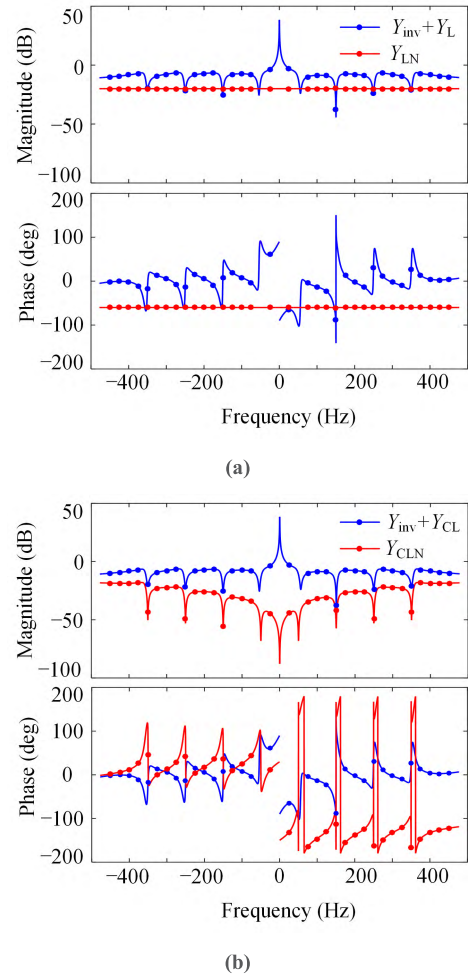

FIGURE 9. Theoretical curves and measurement results for the equivalent admittances (solid lines: theoretical calculation results; dots: experimentally measured results). (a) Admittances without the imbalance compensation. (b) Admittances with the imbalance compensation.

In Fig. 9, the theoretical values for different admittances are presented as solid lines, and the measured values of the admittances are represented by the dots. It can be seen that the measured values of the admittances match the values of the theoretical curves. Moreover, a comparison of the compensated coupled-admittance Y_{CLN} with the uncompensated coupled-admittance Y_{LN} clearly reveals that the imbalance compensation significantly decreases the magnitude of the coupled-admittance, especially at the frequencies with resonant controllers (i.e. $\pm 3^{th}$, $\pm 5^{th}$ and $\pm 7^{th}$ harmonic frequencies). Accordingly, it can be proven that the active compensation of the MFGCI can mitigate the imbalance of the system caused by the unbalanced load. The equivalent balanced admittances of the three-phase system ($Y_{inv} + Y_L$ and $Y_{inv} + Y_{CL}$) are not affected by the

imbalance compensation. However, it should be noted that the change of the magnitude-frequency and phase-frequency characteristics of the coupled-admittance can affect the small-signal stability of the system, which is analyzed in the next section.

IV. COMPLEX SPACE VECTOR-BASED SMALL-SIGNAL STABILITY ANALYSIS FOR THE THREE-PHASE SYSTEM
A. SMALL-SIGNAL STABILITY ANALYSIS METHOD
As illustrated in Fig. 4, when the three-phase system with unbalanced load is connected to the grid without the grid-impedance, the unbalanced load current component at the frequency $-\omega_e$ is decoupled from the circuit at the frequency ω_e. However, the grid-impedance commonly exists in practice, particularly in weak grid condition. In this situation, the circuit at the frequency ω_e and the circuit at the frequency $-\omega_e$ are coupled due to the coupled-admittance Y_{LN}, which can be observed in Fig. 10.
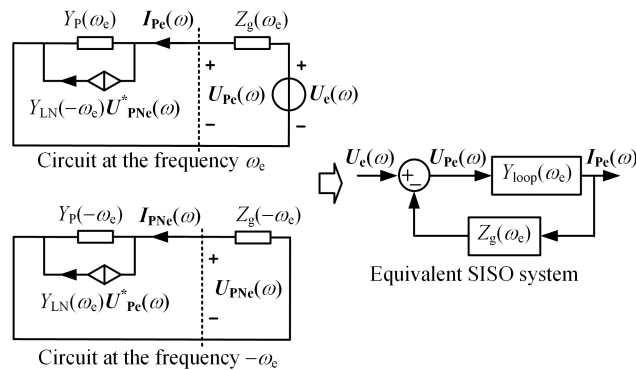
FIGURE 10. Diagram of the coupling between the circuit at the frequency ω_e and the circuit at the frequency $-\omega_e$.

The diagram in Fig. 10 reveals that due to the grid-impedance Z_g and the unbalanced load current at the frequency $-\omega_e$, the voltage U_{PNe} at the frequency $-\omega_e$ is introduced at the PCC. As a result, the additional current component is introduced into the circuit at the frequency ω_e by the coupled-admittance and can be derived as $Y_{LN}(-\omega_e)U^*_{PNe}(\omega)$. In Fig. 10, $Y_P(\omega_e) = Y_{inv}(\omega_e) + Y_L(\omega_e)$. $Z_g(\omega_e)$ is the grid-impedance. In the circuit at the frequency $-\omega_e$, the admittance and the grid-impedance are expressed as $Y_P(-\omega_e)$, and $Z_g(-\omega_e)$.

Based on the model shown in Fig. 10, an equivalent SISO system ($U_e(\omega)$ is the input, $I_{Pe}(\omega)$ is the output.) can be obtained taking the coupling between the circuits at ω_e and $-\omega_e$ into account [10]. Furthermore, the equivalent admittance of the three-phase system considering the grid-impedance can be derived based on (5), (6), and (15) as follows:

$$Y_{loop}(\omega_e) = \frac{I_{Pe}(\omega)}{U_{Pe}(\omega)} = \left[Y_P(\omega_e) - Y_{LN}(-\omega_e)Y^*_{LN}(\omega_e) \right.$$
$$\left. \times \frac{Z^*_g(-\omega_e)}{1 + Z^*_g(-\omega_e)Y^*_P(-\omega_e)} \right] \quad (33)$$

The stability of the proposed SISO equivalent system can be analyzed based on the Nyquist curve of $Z_g(\omega_e)Y_{loop}(\omega_e)$ [6]. For the complex space vector based model, the system is asymptotically stable if the Nyquist curve of $Z_g(\omega_e)Y_{loop}(\omega_e)$ does not encircle -1 for $-\infty < \omega_e < +\infty$ [16].

B. STABILITY ANALYSIS CONSIDERING THE GRID-IMPEDANCE AND THE IMBALANCE COMPENSATION
Based on the small-signal stability analysis method, the stability of the MFGCI system with unbalanced load is investigated. Considering the grid-impedance as three-phase balanced inductance L_g, the expression of $Z_g(\omega_e)$ is

$$Z_g(\omega_e) = j\omega_e L_g \quad (34)$$

The parameters of the system are listed in Table I. The small-signal stability analysis is conducted in three scenarios:
  A) $L_g = 0.1$mH. The imbalance of the local load is not compensated. $Y_L(\omega_e)$, $Y_{LN}(\omega_e)$, and $Y_{inv}(\omega_e)$ can be obtained based on (5), (6), and (15). The Nyquist curve of $Z_g(\omega_e)Y_{loop}(\omega_e)$ is shown in Fig. 11(a).
  B) $L_g = 1.8$mH. The imbalance of the local load is not compensated. $Y_L(\omega_e)$, $Y_{LN}(\omega_e)$, and $Y_{inv}(\omega_e)$ are the same as the admittances in scenario A. The Nyquist curve of $Z_g(\omega_e)Y_{loop}(\omega_e)$ is shown in Fig. 11(b).
  C) $L_g = 1.8$mH. The unbalanced local load is compensated by the MFGCI based on the proposed compensation algorithm. In this scenario, $Y_{loop}(\omega_e)$ can be obtained by using $Y_{CL}(\omega_e)$ and $Y_{CLN}(\omega_e)$ to replace $Y_L(\omega_e)$ and $Y_{LN}(\omega_e)$ in (33). $Y_{CL}(\omega_e)$ and $Y_{CLN}(\omega_e)$ can be obtained based on (29) and (30). The Nyquist curve of $Z_g(\omega_e)Y_{loop}(\omega_e)$ is illustrated in Fig. 11(c).

In scenario A, the magnitude of $Z_g(\omega_e)$ is close to 0, especially within the control bandwidth of the current control loop (hundreds of Hertz). Thus, the coupling between the circuits at ω_e and $-\omega_e$ is weak in this situation. As shown in Fig. 11(a), the Nyquist curve of $Z_g(\omega_e)Y_{loop}(\omega_e)$ is far away from the $(-1, 0)$, which means the system is stable.

In scenario B, while the grid-impedance increases, the coupling between the circuits caused by the unbalanced load is strengthened. As illustrated in Fig. 11(b), when $L_g = 1.8$mH, the system is unstable because the Nyquist curve of $Z_g(\omega_e)Y_{loop}(\omega_e)$ encircles the $(-1, 0)$.

In scenario C, by adopting the proposed imbalance compensation algorithm, the magnitude of the coupled-admittance is decreased as shown in Fig. 9(b). Thus, the coupling between the circuit at ω_e and the circuit at $-\omega_e$ is attenuated. Therefore, as illustrated in Fig. 11(c), the system becomes stable in this situation while the L_g is still equal to 1.8mH.
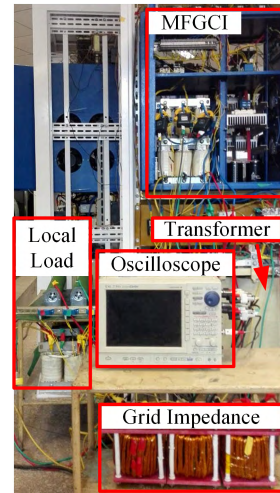
V. EXPERIMENTAL RESULTS
To verify the stability analysis presented in Section IV, the experimental platform is built according to the circuit topology displayed in Fig. 1. The control system of the MFGCI
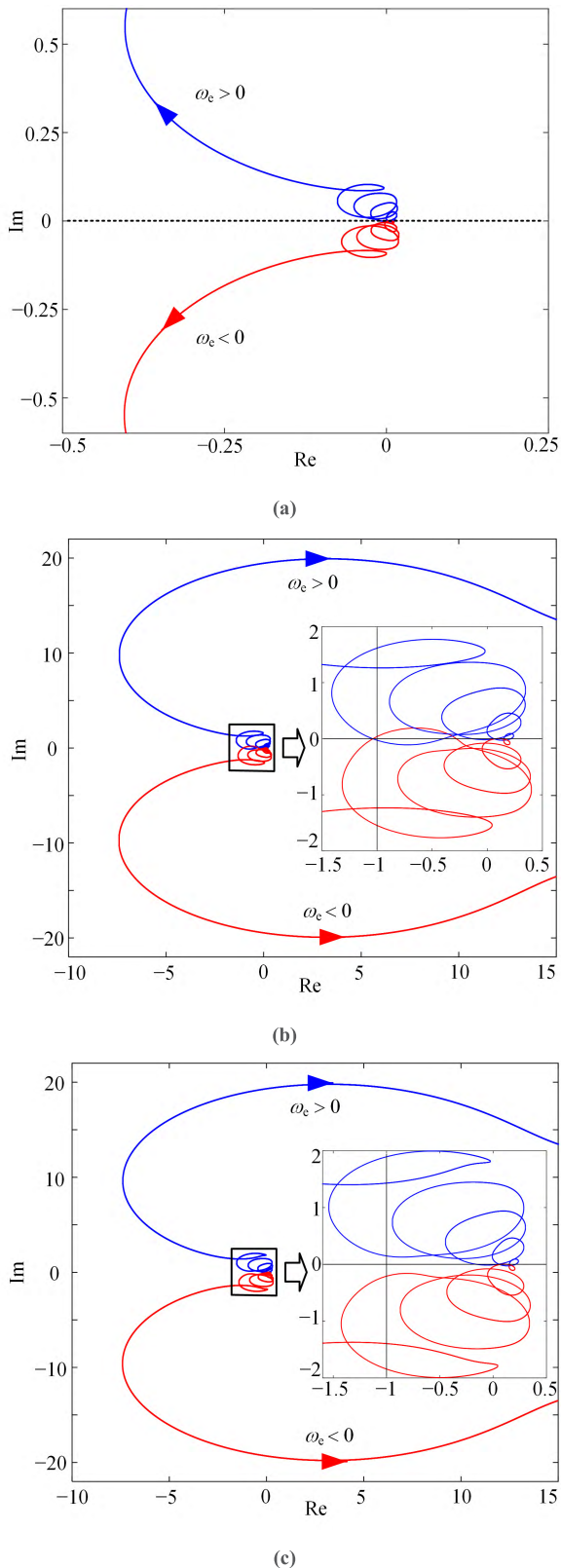
FIGURE 11. Stability analysis for the three-phase system. (a) The unbalanced load is not compensated ($L_g = 0.1$mH). (b) The unbalanced load is not compensated ($L_g = 1.8$mH). (c) The unbalanced load is compensated by the MFGCI($L_g = 1.8$mH).

is implemented in the DSP processor TMS320F28335. The experimental parameters of the MFGCI and the local load are the same as the parameters used for theoretical analysis which are listed in Table I. In practice, the MFGCI and the unbalanced local load are connected to the local distribution grid through a 130V/400V step-up transformer. Also, a three-phase inductor is used as the equivalent grid-impedance. The experimental setup is shown in Fig. 12.

**FIGURE 12.** The experimental setup.

Three experiments, corresponding to the stability analysis scenarios presented in Section IV.B, are conducted to verify the analysis results. The experimental results are presented in Fig 13.

The waveforms of I_{inv} (three-phase output-current of the MFGCI), I_P (three-phase current of PCC), and U_P (three-phase voltage of PCC) are presented for different scenarios in Fig. 13.

The experimental results for the scenario A are presented in Fig. 13(a). Since the unbalanced load is not compensated, I_P is three-phase unbalanced, even though the output-current of the MFGCI is balanced. Except for the unbalanced current at the negative fundamental frequency, few harmonic components exist in the waveforms of I_{inv}, I_P and U_P. Thus, the three-phase system is stable when $L_g = 0.1$mH.

The experimental results for the scenario B are shown in Fig. 13(b). The results reveal that when L_g is increased to 1.8mH, serious harmonic distortions for both currents and voltages of the three-phase system arise, which indicates that the system is unstable.
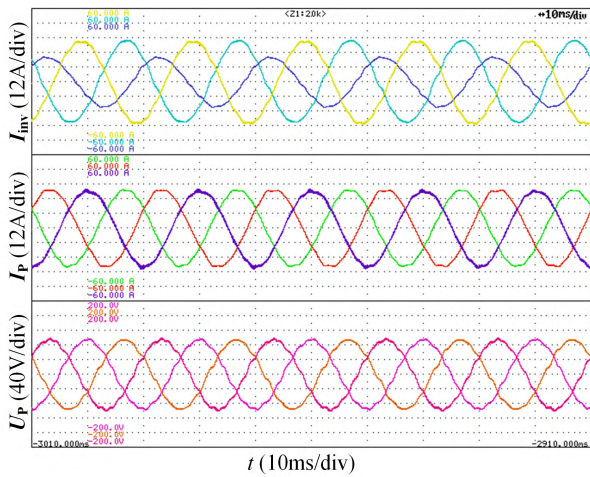
The experimental results for the scenario C are shown in Fig. 13(c). When the L_g is still equal to 1.8mH, the proposed imbalance compensation algorithm of the MFGCI is adopted. The results indicate that the imbalance of I_P is clearly reduced. Moreover, the harmonic distortion of the system is significantly decreased which confirms that the system is stable.
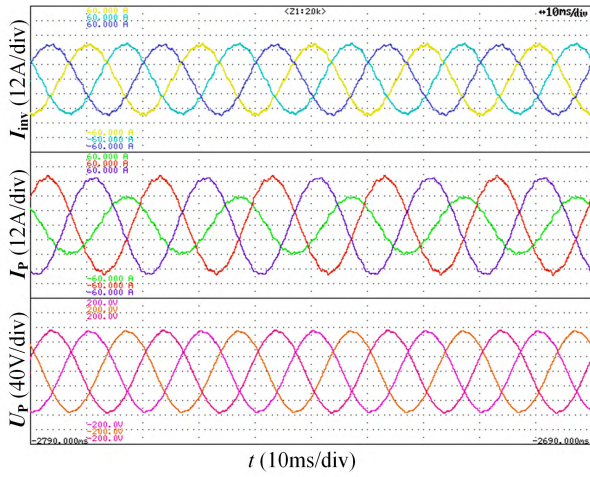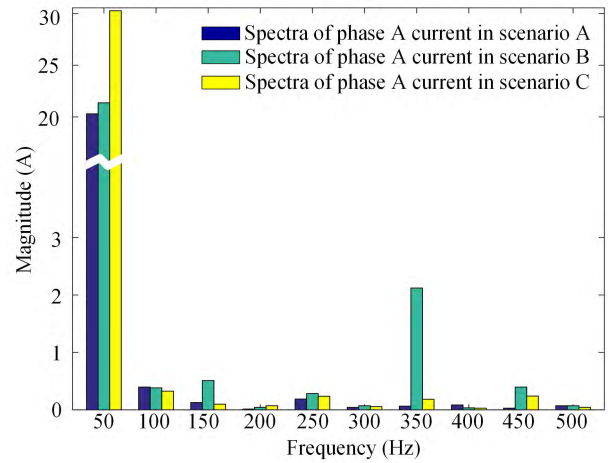
(a)
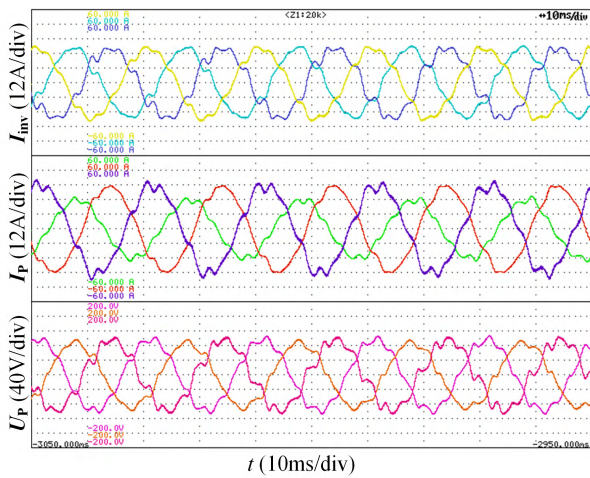
(b)

(c)

FIGURE 13. Experimental results for the three-phase system. (a) The unbalanced load is not compensated ($L_g = 0.1mH$). (b) The unbalanced load is not compensated ($L_g = 1.8mH$). (c) The unbalanced load is compensated by the MFGCI ($L_g = 1.8mH$).

FIGURE 14. Harmonic spectra for the phase A current of I_P in different scenarios.

To better illustrate the small-signal stability in the different scenarios, the harmonic spectra for the phase A current of I_P in three scenarios are obtained based on the Fast-Fourier-Transform (FFT) analysis. The harmonic spectra are displayed in Fig. 14. The spectra show that when the imbalance compensation algorithm is adopted, the phase A current of I_P at the fundamental frequency is increased. Thus, as shown in Fig. 13(c), the balanced I_P can be achieved. When the system is unstable, the harmonic components of the phase current rise significantly.

VI. CONCLUSION

In this paper, the complex space vector based small-signal impedance model is proposed for the three-phase system including the MFGCI and the unbalanced local load. The MFGCI is adopted to realize the power transmission and imbalance distortion compensation in the system.

To achieve the imbalance compensation, a CPT-based active imbalance compensation algorithm is proposed and integrated into the MFGCI. By incorporating the control scheme of the MFGCI and the imbalance of the local load, the impedance model presented in the paper reveals a specific small-signal response feature of the unbalanced three-phase system. Based on the proposed model, the theoretical analysis and impedance measurement results prove that the CPT-based active compensation can attenuate the imbalance of the system by reshaping the equivalent impedance of the compensated load.

In addition, the small-signal stability analysis for the three-phase system is also presented based on the impedance analysis method. The analysis results indicate that the imbalance of the local load can affect the small-signal stability of the three-phase system when the grid-impedance is not negligible. Furthermore, the analysis and experimental results also confirm that the adoption of the proposed imbalance

compensation algorithm can improve the stability of the system by decreasing the coupled-impedance introduced by the unbalanced load.

REFERENCES

[1] Z. Zeng, H. Yang, R. Zhao, and C. Cheng, "Topologies and control strategies of multi-functional grid-connected inverters for power quality enhancement: A comprehensive review," *Renew. Sustain. Energy Rev.*, vol. 24, pp. 223–270, Aug. 2013.

[2] C. Bao, X. Ruan, X. Wang, W. Li, D. Pan, and K. Weng, "Step-by-step controller design for LCL-type grid-connected inverter with capacitor-current-feedback active-damping," *IEEE Trans. Power Electron.*, vol. 29, no. 3, pp. 1239–1253, Mar. 2014.

[3] C. Citro, P. Siano, and C. Cecati, "Designing inverters' current controllers with resonance frequencies cancellation," *IEEE Trans. Ind. Electron.*, vol. 63, no. 5, pp. 3072–3080, May 2016.

[4] M. Abusara, S. Sharkh, and P. Zanchetta, "Control of grid-connected inverters using adaptive repetitive and proportional resonant schemes," *J. Power Electron.*, vol. 15, no. 2, pp. 518–528, Mar. 2015.

[5] M. Liserre, R. Teodorescu, and F. Blaabjerg, "Stability of photovoltaic and wind turbine grid-connected inverters for a large set of grid impedance values," *IEEE Trans. Power Electron.*, vol. 21, no. 1, pp. 263–272, Jan. 2006.

[6] J. Sun, "Impedance-based stability criterion for grid-connected inverters," *IEEE Trans. Power Electron.*, vol. 26, no. 11, pp. 3075–3078, Nov. 2011.

[7] B. Wen, D. Dong, D. Boroyevich, P. Mattavelli, R. Burgos, and Z. Shen, "Impedance-based analysis of grid-synchronization stability for three-phase paralleled converters," *IEEE Trans. Power Electron.*, vol. 31, no. 1, pp. 26–38, Jan. 2016.

[8] M. Cespedes and J. Sun, "Impedance modeling and analysis of grid-connected voltage-source converters," *IEEE Trans. Power Electron.*, vol. 29, no. 3, pp. 1254–1261, Mar. 2014.

[9] X. Wang, L. Harnefors, and F. Blaabjerg, "Unified impedance model of grid-connected voltage-source converters," *IEEE Trans. Power Electron.*, vol. 33, no. 2, pp. 1775–1787, Feb. 2018.

[10] C. Zhang, X. Cai, A. Rygg, and M. Molinas, "Sequence domain SISO equivalent models of a grid-tied voltage source converter system for small-signal stability analysis," *IEEE Trans. Energy Convers.*, vol. 33, no. 2, pp. 741–749, Jun. 2018.

[11] M. Céspedes and J. Sun, "Methods for stability analysis of unbalanced three-phase systems," in *Proc. IEEE Energy Convers. Congr. Expo. (ECCE)*, Raleigh, NC, USA, Sep. 2012, pp. 3090–3097.

[12] A. S. Bubshait, A. Mortezaei, M. G. Simões, and T. D. C. Busarello, "Power quality enhancement for a grid connected wind turbine energy system," *IEEE Trans. Ind. Appl.*, vol. 53, no. 3, pp. 2495–2505, May/Jun. 2017.

[13] A. Mortezaei, C. Lute, M. G. Simões, F. P. Marafão, and A. Boglia, "PQ, DQ and CPT control methods for shunt active compensators— A comparative study," in *Proc. IEEE Energy Convers. Congr. Expo. (ECCE)*, Pittsburgh, PA, USA, Sep. 2014, pp. 2994–3001.

[14] P. Tenti, H. K. M. Paredes, and P. Mattavelli, "Conservative power theory, a framework to approach control and accountability issues in smart microgrids," *IEEE Trans. Power Electron.*, vol. 26, no. 3, pp. 664–673, Mar. 2011.

[15] F. P. Marafão, D. I. Brandão, A. Costabeber, and H. K. M. Paredes, "Multi-task control strategy for grid-tied inverters based on conservative power theory," *IET Renew. Power Gener.*, vol. 9, no. 2, pp. 154–165, 2015.

[16] L. Harnefors, "Modeling of three-phase dynamic systems using complex transfer functions and transfer matrices," *IEEE Trans. Ind. Electron.*, vol. 54, no. 4, pp. 2239–2248, Aug. 2007.

[17] D. I. Brandao, H. K. M. Paredes, A. Costabeber, and F. P. Marafão, "Flexible active compensation based on load conformity factors applied to non-sinusoidal and asymmetrical voltage conditions," *IET Power Electron.*, vol. 9, no. 2, pp. 356–364, 2016.

[18] Z. Zeng, H. Yang, S. Tang, and R. Zhao, "Objective-oriented power quality compensation of multifunctional grid-tied inverters and its application in microgrids," *IEEE Trans. Power Electron.*, vol. 30, no. 3, pp. 1255–1265, Mar. 2015.

WEI JIN was born in Shuozhou, Shanxi, China, in 1990. He received the B.S. degree in electrical engineering from Tianjin University, Tianjin, China, in 2013, where he is currently pursuing the Ph.D. degree with the School of Electrical and Information Engineering.

His research interests include control technology of converters, power quality control of micro-grids and distribution networks, and system stability analysis.

YONGLI LI was born in Shijiazhuang, Hebei, China, in 1963. She received the B.S. and M.S. degrees in electrical engineering from Tianjin University, Tianjin, China, in 1984 and 1987, respectively, and the Ph.D. degree in electrical engineering from the Université Libre de Bruxelles, Brussels, Belgium, in 1993. She is currently a Professor with the School of Electrical and Information Engineering, Tianjin University.

Her research interests include fault analysis of power systems and fault diagnosis of electrical equipment, protection and adaptive reclosing of EHV/UHV transmission systems, protection and control of the micro-grid, and distribution networks.

GUANGYU SUN was born in Shenyang, Liaoning, China, in 1990. He received the B.S. degree in electrical engineering from Tianjin University, Tianjin, China, in 2012 where he is currently pursuing the Ph.D. degree with the School of Electrical and Information Engineering.

His research interests include phase-locked loop and control for power engineering applications, power quality control of the micro-grid, and distribution networks.

XIAOLONG CHEN was born in Puyang, Henan, China, in 1985. He received the B.S., M.S., and Ph.D. degrees in electrical engineering from Tianjin University, Tianjin, China, in 2010, 2012, and 2015, respectively. He is currently a Lecturer with the School of Electrical and Information Engineering, Tianjin University.

His research interests include protection and control of the micro-grid, distribution networks, and EHV/UHV transmission systems.

YAN GAO was born in Hengshui, Hebei, China, in 1995. He received the B.S. degree in electrical engineering from Tianjin University, Tianjin, China, in 2017, where he is currently pursuing the M.S. degree with the School of Electrical and Information Engineering.

His research interests include protection and control of the micro-grid, and distribution networks.

● ● ●